
Research Article: New Research | Sensory and Motor Systems

Foreground-Background Segmentation Revealed during Natural Image Viewing

Paolo Papale¹, Andrea Leo¹, Luca Cecchetti¹, Giacomo Handjaras¹, Kendrick N. Kay², Pietro Pietrini¹ and Emiliano Ricciardi¹

¹*Molecular Mind Lab, IMT School for Advanced Studies Lucca, Lucca 55100, Italy*

²*Center for Magnetic Resonance Research, Department of Radiology, University of Minnesota, Twin Cities, Minneapolis, MN 55455, USA*

DOI: 10.1523/ENEURO.0075-18.2018

Received: 19 February 2018

Revised: 15 May 2018

Accepted: 15 May 2018

Published: 28 June 2018

Author contributions: P.P.: designed research, analyzed data and wrote the paper. A.L., L.C., G.H., P.Pietrini and E.R.: designed research and wrote the paper. K.K.: designed research, performed research and wrote the paper.

Conflict of Interest: Authors report no conflict of interest.

Correspondence address: Emiliano Ricciardi, E-mail: emiliano.ricciardi@imtlucca.it

Cite as: eNeuro 2018; 10.1523/ENEURO.0075-18.2018

Alerts: Sign up at eneuro.org/alerts to receive customized email alerts when the fully formatted version of this article is published.

Accepted manuscripts are peer-reviewed but have not been through the copyediting, formatting, or proofreading process.

Copyright © 2018 Papale et al.

This is an open-access article distributed under the terms of the Creative Commons Attribution 4.0 International license, which permits unrestricted use, distribution and reproduction in any medium provided that the original work is properly attributed.

1. **Title:** Foreground-background segmentation revealed during natural image viewing
2. **Abbreviated Title:** Scene segmentation of natural images in humans
3. **Authors and affiliations:** Paolo Papale¹, Andrea Leo¹, Luca Cecchetti¹, Giacomo Handjaras¹, Kendrick Kay², Pietro Pietrini¹ and Emiliano Ricciardi¹ (1. Molecular Mind Lab, IMT School for Advanced Studies Lucca, Lucca, 55100 Italy; 2. Center for Magnetic Resonance Research, Department of Radiology, University of Minnesota, Twin Cities, Minneapolis, MN, 55455, USA)
4. **Author Contributions:** P.P.: designed research, analyzed data and wrote the paper. A.L., L.C., G.H., P.Pietrini and E.R: designed research and wrote the paper. K.K.: designed research, performed research and wrote the paper.
5. **Correspondence should be addressed to:** Emiliano Ricciardi (emiliano.ricciardi@imtlucca.it)
6. **Number of Figures:** 5
7. **Number of Tables:** 2
9. **Number of words for Abstract:** 181
10. **Number of words for Significance Statement:** 120
11. **Number of words for Introduction:** 684
12. **Number of words for Discussion:** 1729
14. **Conflict of Interest:** Authors report no conflict of interest

1 **Abstract**

2 One of the major challenges in visual neuroscience is represented by foreground-
3 background segmentation. Data from nonhuman primates show that segmentation leads to
4 two distinct, but associated processes: the enhancement of neural activity during figure
5 processing (i.e., foreground enhancement) and the suppression of background-related activity
6 (i.e., background suppression). To study foreground-background segmentation in ecological
7 conditions, we introduce a novel method based on parametric modulation of low-level image
8 properties followed by application of simple computational image-processing models. By
9 correlating the outcome of this procedure with human fMRI activity, measured during passive
10 viewing of 334 natural images, we produced easily interpretable “correlation images” from
11 visual populations. Results show evidence of foreground enhancement in all tested regions,
12 from V1 to LOC, while background suppression occurs in V4 and LOC only. “Correlation
13 images” derived from V4 and LOC revealed a preserved spatial resolution of foreground
14 textures, indicating a richer representation of the salient part of natural images, rather than a
15 simplistic model of object shape. Our results indicate that scene segmentation occurs during
16 natural viewing, even when individuals are not required to perform any particular task.

17 18 **Significance Statement**

19 Foreground-background segmentation has been considered critical to form discrete
20 object representations from continuous sensory percepts. We developed a pre-filtering
21 approach which overcame typical limitations in modeling brain responses to complex stimuli
22 and could be generalized to related processes. Our findings provide novel support to the
23 hypothesis that foreground-background segmentation of natural scenes occurs during passive
24 perception, sustained by the distributed activity of multiple areas across the visual processing
25 stream. Specifically, while foreground information is enhanced along the entire visual

26 pathway, V4 and LOC show a background suppression effect, though retaining texture
27 information from the foreground. Our observations challenge the idea that these regions of
28 the visual system may primarily encode simple object representations based on silhouette or
29 shape features only.

30

31 **Introduction**

32 In the scientific journey toward a satisfying understanding of the human visual system,
33 scene segmentation represents a central problem “for which no theoretical solution exists”
34 (Wu et al., 2006). Segmentation into foreground and background is crucial to make sense of
35 the surrounding visual environment, and its pivotal role as an initial step of visual content
36 identification has long been theorized (Biederman, 1987). Indeed, according to Fowlkes and
37 colleagues (2007), humans can produce consistent segmentations of natural images. However,
38 even though more recent approaches based on deep convolutional networks produced
39 promising results (He et al., 2017), both the computational and neurophysiological processes
40 that underlie scene segmentation are still a matter of debate.

41 To date, numerous studies found evidence of texture segmentation and figure-ground
42 organization in the early visual cortex of nonhuman primates (Lamme, 1995; Lee et al., 1998;
43 Poort et al., 2012; Self et al., 2013) and humans (Kastner et al., 2000; Scholte et al., 2008; Kok
44 and de Lange, 2014). It has been showed that the identification of salient visual attributes
45 arises from a region-filling mechanism, that targets neural populations mapping relevant
46 points in space (Roelfsema, 2006). In particular, a recent study on monkeys attending
47 artificial stimuli revealed an early enhancement of V1 and V4 neurons when their receptive
48 fields covered the foreground, and a later response suppression when their receptive fields
49 were located in the stimulus background (Poort et al., 2016) – extending results from a
50 previous study (Lamme et al., 1999). Thus the primate brain groups together image elements

51 which belong to the figure, showing an enhanced activity for the foreground and a concurrent
52 suppression of the background.

53 However, from an experimental viewpoint, the role of figure-ground segmentation has
54 primarily been demonstrated by means of non-ecological stimuli (e.g., binary figures, random
55 dots, oriented line segments and textures). It should be noted that previous reports
56 demonstrated how models of brain responses to artificial stimuli are suboptimal in predicting
57 responses to natural images (David et al., 2004; Felsen and Dan, 2005). Although two recent
58 studies investigated border-ownership in monkeys with both artificial and natural stimuli
59 (Hesse and Tsao, 2016; Williford and von der Heydt, 2016), a proof of the occurrence of
60 foreground-background segmentation in the human brain during visual processing of
61 naturalistic stimuli (e.g., natural images and movies) is still lacking. This pushes towards the
62 development of novel methods specifically designed for testing segmentation in ecological
63 conditions.

64 In light of this, we investigated foreground enhancement and background suppression,
65 as specific processes involved in scene segmentation during passive viewing of natural images.
66 We used fMRI data, previously published by Kay and colleagues (Kay et al., 2008), to study
67 brain activity patterns from seven visual regions of interest (ROIs): V1, V2, V3, V3A, V3B, V4
68 and lateral occipital complex (LOC) in response to 334 natural images, whose “ground-truth”
69 segmented counterparts have been included in the Berkeley Segmentation Dataset (BSD)
70 (Arbelaez et al., 2011).

71 To this aim, we developed a novel pre-filtering modeling approach to study brain
72 responses to complex, natural images without relying on explicit models of scene
73 segmentation, and adopting a validated and biologically plausible description of activity in
74 visual cortices. Our method is similar to other approaches where explicit computations are
75 performed on representational features, rather than on the original stimuli (Naselaris et al.,
76 2011). For instance, these methods have been recently used to investigate semantic

77 representation (e.g. Huth et al., 2012; Handjaras et al., 2017) or boundary and surface-related
78 features (Lescroart et al., 2016). However, as opposed to the standard modeling framework –
79 according to which alternative models are computed from the stimuli to predict brain
80 responses – here, low-level features of the stimuli are parametrically modulated and simple
81 descriptors of each filtered image (i.e., edges position, size and orientation) are aggregated in
82 a fixed model (Figure 1). The correspondence between the fixed model and fMRI
83 representational geometry related to intact images, was then evaluated using
84 representational similarity analysis (RSA) (Kriegeskorte et al., 2008). Notably, this approach
85 can also be exploited to obtain highly informative “correlation images” representing the
86 putative computations of different brain regions and may be generalized to investigate
87 different phenomena in visual neuroscience.

88

89 *** Insert Figure 1 near here ***

90

91 **Materials and Methods**

92 To assess differences between cortical processes involved in foreground-background
93 segmentation, we employed a low-level description of images, defined by a weighted sum of
94 the representational dissimilarity matrices (RDMs) of four well-known computational models
95 (Figure 2D). These models are based on simple features – edge position, size and orientation –
96 whose physiological counterparts are well known (Marr, 1982). The model was kept constant
97 while the images were parametrically filtered and iteratively correlated with representational
98 measures of brain activity through RSA. For each ROI, this pre-filtering modeling approach led
99 to a pictorial and easily interpretable representation of the optimal features (contrast and
100 spatial frequencies) of foreground and background of natural images (i.e., “correlation
101 images”). The analytical pipeline is schematized in Figure 2.

102

103 *** Insert Figure 2 near here ***

104

105 **Stimuli and behavioral segmentation of foreground and background.**

106 We selected from the 1870 images used by (Kay et al., 2008) a sub-sample of 334
107 pictorial stimuli which are also represented in the Berkeley Segmentation Dataset 500 (BSD)
108 (Arbelaez et al., 2011). For each BSD image, 5-7 subjects manually performed an individual
109 “ground-truth” segmentation, which is provided by the authors of the dataset

110 (<http://www.eecs.berkeley.edu/Research/Projects/CS/vision/grouping/resources.html>).

111 Although figure-ground judgment is rather stable across subjects (Fowlkes et al., 2007), we
112 selected the largest patch - manually labeled as foreground - among the behavioral
113 segmentations, in order to build a foreground binary mask. For each image, this mask was
114 then down-sampled and applied to the original stimulus to isolate the foreground and the
115 background pixels (Kay et al., 2008).

116

117 **fMRI Data.**

118 The fMRI data used in this study are publicly available at [http://crcns.org/data-](http://crcns.org/data-sets/vc/vim-1)
119 [sets/vc/vim-1](http://crcns.org/data-sets/vc/vim-1) (Kay et al., 2011). Two subjects (Males, age: 33 and 25) were acquired using
120 the following MRI parameters: 4T INOVA MR, matrix size 64x64, TR 1s, TE 28ms, flip angle
121 20°, spatial resolution 2 x 2 x 2.5 mm³. For each subject five scanning sessions (7 runs each)
122 were performed on five separate days. The stimuli were 1870 greyscale natural images with
123 diameter 20° (500px), embedded in a grey background, and were presented for 1s, flickering
124 at 5Hz, with an ISI of 3s. Subjects were asked to fixate a central white square of 0.2°(4px).

125 Seven visual regions of interest (ROIs) - V1, V2, V3, V3A, V3B, V4 and LOC - were defined and
126 brain activity patterns related to stimulus presentation was extracted from these regions. For

127 additional details on pre-processing, retinotopic mapping and ROIs localization, please refer
128 to (Kay et al., 2008).

129

130 **Computational Models.**

131 In accordance with a previous fMRI study that, to the best of our knowledge, has tested
132 the highest number of computational models, we selected four untrained models: two
133 showing highest correlations with brain activity patterns in early visual areas, and the others,
134 showing highest correlations with LOC (Khaligh-Razavi and Kriegeskorte, 2014). All these
135 models are based on biologically inspired features, such as Gabor filters and image gradient
136 and comprise: GIST (Oliva and Torralba, 2001), Dense SIFT (Lazebnik et al., 2006), Pyramid
137 Histograms of Gradients (PHOG) (Bosch et al., 2007) and Local Binary Patterns (LBP) (Ojala
138 et al., 2001). For an exhaustive description of the four models – and links to Matlab codes –
139 see the work by Khaligh-Razavi (2014) and Khaligh-Razavi and Kriegeskorte (2014). Our
140 model choice was also motivated by the fact that the stimuli were grayscale and had a fixed
141 circular aperture. Thus, we excluded descriptions based on color or silhouette information, as
142 well as pre-trained convolutional neural networks which are biased towards the global shape
143 of the image (Kubilius et al., 2016).

144

145 **Representational Similarity Analysis (RSA).**

146 For each filtered image, we collected feature vectors from the four computational
147 models (PHOG, GIST, LBP and Dense SIFT), and RDMs were then obtained (1 minus the
148 Pearson correlation metric). These four RDMs were normalized in a range between 0 and 1,
149 and combined to obtain the fixed biologically plausible model of the stimuli (for a graphical
150 representation of the process, see Figure 2D). The four model RDMs were combined through a
151 weighted sum, based on an estimation of their correlation with the representational model of
152 brain activity. Single subject RDMs were similarly computed using fMRI activity patterns for

153 each of the seven ROIs, and then averaged across the two subjects. We used Spearman's rho
154 (ρ) to assess the correlation between the RDM from each step of the image filtering
155 procedures and the RDM of each brain ROI. To obtain unbiased estimations of the correlation
156 between models and fMRI, a 5-fold cross-validation procedure based on a weighted sum of
157 the models was developed: model weights were first estimated through linear regression on a
158 portion (80%) of the RDMs, and the correlation with fMRI data was then computed based on
159 the remainder of the RDMs (20%). The correlation values derived from this procedure were
160 averaged across the five folds, to obtain a unique estimate of the similarity between image
161 features and brain activity. This analysis was performed independently in each of the seven
162 ROIs, and the standard error for each correlation value was estimated with bootstrapping of
163 the stimuli – 1,000 iterations (Efron and Tibshirani, 1993).

164 In addition, as each ROI may show a distinct signal-to-noise ratio, we computed a noise
165 estimation by correlating the brain RDMs extracted from the two subjects. This procedure
166 allows for qualitative comparison between different ROIs and could help in estimate how well
167 each model explains fMRI RDMs given the noise in the data.

168

169 **Foreground enhancement testing**

170 A permutation test was performed to statistically assess the enhancement of the
171 information retained in the behaviorally segmented foreground. In this test both the “fovea-to-
172 periphery” bias that characterizes natural images, and possible differences in contrast
173 between foreground and background were controlled (Figure 2A). For each iteration, the 334
174 foreground masks were shuffled and a random foreground segmentation was associated to
175 each stimulus. The RMS contrast of each obtained segmented image was matched to that of
176 the behaviorally segmented counterpart. Of note, this set of randomly-segmented images had
177 the same distribution of masked portions of the visual field as the one from the behavioral
178 segmentation, so the same amount of information was isolated at each permutation step. This

179 procedure was repeated 1,000 times, to build a null distribution of alternative segmentations:
180 four examples of random segmentation are shown in Figure 2A. For each permutation step,
181 features were extracted from each randomly segmented image and RSA was performed using
182 the procedure described above.

183

184 **Parametric filtering procedures.**

185 In order to investigate differential processing of foreground and background in the
186 visual system, we employed three different filtering procedures (contrast - through alpha
187 channel modulation - low- and high-pass filtering of spatial frequencies) applied
188 parametrically (4 steps each) to the foreground or the background. For each filtering
189 procedure, the four manipulated images are represented in Figure 2C. For low- and high-pass
190 filtering, we employed a Butterworth filter (5th order), linearly sampling from a log-
191 transformed distribution of frequencies ranging from 0.05 to 25 cyc/°, while keeping the RMS
192 contrast fixed.

193

194 **Background suppression testing.**

195 To test background suppression, we performed a two-tailed permutation test. In each
196 ROI, we computed the difference between the correlation of the intact version of the stimuli
197 and each step of the background filtering procedures (Figure 2B). Afterwards, a permutation
198 test (10,000 iterations) was performed by random sampling two groups from the bootstrap
199 distributions, obtaining a null distribution of correlation differences. Reported results are
200 Bonferroni corrected (for the 13 comparisons in each ROI).

201

202 **Correlation images.**

203 For each ROI, the effects of the filtering procedures were combined, to build
204 “correlation images”. To this aim we used the filtering step with the highest correlation

205 between the fixed model and RDMs from fMRI data, for foreground and background
206 respectively. In detail, we averaged the best images for the low- and high-pass filters, and
207 multiplied each pixel for the preferred alpha-channel value (contrast).

208

209 **Significance testing.**

210 To assess the statistical significance of the correlations obtained with RSA in all the
211 above mentioned filtering procedures, we built a robust ROI-specific permutation test (1,000
212 iterations), by randomly sampling voxels of the occipital lobe not located in any of the seven
213 ROIs. We labeled these voxels as ‘control-voxels’. This procedure has the advantage to be
214 resilient to biases in fMRI data (Schreiber and Krekelberg, 2013), instead of simply taking into
215 account the distribution of the RDM values, as in (Khaligh-Razavi and Kriegeskorte, 2014). In
216 addition, the procedure that we developed is also useful to control for the effects related to
217 number of voxels and to the signal-to-noise ratio of each ROI.

218 First, for each ROI we computed the standard error of the ROI-specific noise estimation
219 with bootstrap resampling of the stimuli (1,000 iterations). Second, a number of control
220 voxels equal to the number of voxels was randomly selected within each ROI, and the activity
221 of these control voxels in response to the stimuli were used to build a null RDM. Third, the
222 correlation between the null RDMs of the two subjects was computed. However, since we
223 aimed at matching the signal-to-noise ratio of the null distribution to that of each ROI, the null
224 RDM was counted as a valid permutation only if the single subject RDMs correlated to each
225 other within a specific range (i.e., ROI-specific noise estimation \pm standard error). Finally, for
226 each step of the filtering procedures, each of the 1,000 ROI-specific null RDMs were correlated
227 with the fixed model RDM to obtain a null distribution of 1,000 ρ values. A one-tailed rank test
228 was used to assess the significance of the ρ of the fixed model with brain RDMs. For each ROI,
229 we controlled for multiple comparisons (27 tests), through Bonferroni correction.

230 **Code accessibility**

231 All analyses have been implemented in Matlab (The Mathworks Inc.) using in-house
232 developed code (available at the following link: <https://bit.ly/2rC27hY>).

233

234 **Results**

235 Foreground enhancement and background suppression can be tested in ecological
236 conditions following a simple argument: when attempting to predict brain activity of a visual
237 ROI with a specific model, the goodness-of-fit depends on the model inputs, e.g., the spatial
238 information provided. Thus, the correlation between filtered images and fMRI
239 representational patterns evoked by their intact counterpart can be used to verify specific
240 hypotheses on visual processing (Figure 2). In this study, we posit that evidence of
241 preferential processing (i.e., enhancement) should depend on the shape of the foreground
242 instead of the size, the location or the contrast of the segmented region processed through the
243 model. In this regard, a random sampling procedure of foreground segmentations across
244 stimuli would offer a proper choice to account for all these aspects, ultimately testing whether
245 behavioral segmentations provide a better prior for enhancement. On the other hand,
246 background filtering can lead either to a decay or an increase in correlation with brain
247 representational patterns. The former indicates that background-related information is – at
248 least to some extent – processed, whereas the latter denotes that background information is
249 suppressed, since embedding it in the model is not different from adding noise.

250

251 **Comparison of intact and behaviorally segmented images**

252 The correlation between RDMs computed using the fMRI patterns from each of the
253 seven visual ROIs and three descriptions of the stimuli (intact, isolated background and
254 isolated foreground) were tested (Figure 3 and Table 1). Results show significant correlations
255 ($p < 0.05$ Bonferroni corrected) between the intact description of images and fMRI RDMs in

256 V1, V2 and V3. The segmented foreground RDM shows a significant correlation in V2, V4 and
257 LOC, while the segmented background achieves significant correlations in V1 and V2 only. Of
258 note, the correlation yielded by one of the descriptions approaches the ROI-specific SNR
259 estimation (i.e., the maximum reachable correlation given the noise of the data), thus
260 confirming the validity of the fixed model employed (Wu et al., 2006).

261

262 *** Insert Table 1 near here ***

263

264 *** Insert Figure 3 near here ***

265

266 **Foreground is enhanced in all the tested regions**

267 We tested whether the behavioral foreground segmentation from BSD represented a
268 better predictor of RDMs derived from fMRI activity, as compared to alternate configurations
269 obtained by shuffling the segmentation patterns across stimuli (Figure 2A). The correct
270 foreground configuration yielded a significantly higher correlation as compared to the
271 examples from the shuffled dataset (i.e., a null distribution obtained with a permutation test),
272 thus suggesting that the enhancement of foreground-related information occurs during
273 passive perception of natural stimuli in all the tested ROIs (V1: $p = 0.006$; V2: $p < 0.001$; V3: p
274 $= 0.014$; V3A: $p = 0.002$; V3B: $p = 0.005$; V4: $p < 0.001$; LOC: $p < 0.001$).

275 In addition, this analysis rules out two potential confounding effects. One related to a
276 "fovea-to-periphery bias" in our image set. In fact, as already observed in literature, natural
277 images are typically characterized by objects located at the center of the scene - see for
278 instance the object location bias represented in figure 3B in (Alexe et al., 2010). However,
279 since the spatial distribution and number of pixels were kept constant at each permutation
280 step, we replicated the same "fovea-to-periphery bias" in the null distribution. The other
281 confound was related to potential differences in contrast between foreground and

282 background. To account for this, in the permutation test, we matched the root mean square
283 (RMS) contrast of each random segmentation to that of the “ground truth” segmentation
284 obtained from BSD. Overall, these control procedures minimize the chance that the observed
285 enhancement is driven by location, size or contrast of the foreground.

286

287 **Background suppression occurs in higher cortical areas**

288 As the correlation between the background RDM and RDM derived from fMRI activity
289 is significant in V1 and V2 only (Figure 3), we hypothesized that background-related
290 information is suppressed in “higher” visual cortices. Notably, Poort and colleagues (2016)
291 described background suppression as a different, but associated, phenomenon with respect to
292 foreground enhancement. Thus, in order to better characterize where and how background
293 suppression occurs in humans attending to natural images, a further analysis was performed
294 by parametrically filtering out the background of each image, varying its contrast or spatial
295 frequencies (low- and high-pass filtering; Figure 2C). As the correlation between the
296 representational model of V3A, V3B and those derived from intact, isolated foreground and
297 isolated background images is not significant ($p > 0.05$ Bonferroni corrected), these ROIs
298 were not further investigated.

299 When comparing the correlation value of the intact version of the stimuli and the
300 correlation value of each background filtering step, we found that V1, V2 and V3 show a
301 progressive decay, indicating that the background is actually processed by these regions ($p <$
302 0.05 , Bonferroni corrected). On the other hand, in V4 and LOC filtering the background
303 produces significantly higher correlations ($p < 0.05$ Bonferroni corrected), thus indicating
304 that background information is not different from noise (Figure 4). These findings suggest
305 that background suppression is actually performed by higher cortical areas, as also depicted
306 in correlation images (Figure 5).

307 Of note, to validate the proposed method, we performed a simulation of the fMRI
308 experiment using a fully connected layer of a pre-trained convolutional neural network
309 (AlexNet fc6, (Krizhevsky et al., 2012)). The RDM correlation between each contrast filtering
310 step and the representational geometry from the net (i.e., responses to intact images) was
311 computed as in the fMRI analyses (i.e., fixed model). Then, we assessed ground truth
312 computation of the net by showing it the images at each filtering level, thus checking its
313 sensitivity to background manipulation. Results (not shown) demonstrate that our pre-
314 filtering modeling approach correctly reveals the ground-truth computation of the net.

315

316 * Insert Figure 4 near here *

317

318 * Insert Figure 5 near here *

319

320 * Insert Table 2 near here *

321

322 Discussion

323 In the present study, we illustrated how the manipulation of low-level properties of
324 natural images, and the following correlation with patterns of brain responses during passive
325 viewing of the intact stimuli, could disclose the behavior of different regions along the visual
326 pathway.

327 Employing this pre-filtering modeling approach, we tested whether scene
328 segmentation is an automatic process that occurs during passive perception in naturalistic
329 conditions, even when individuals are not required to perform any particular tasks, or to
330 focus on any specific aspect of images. Here, we were able to collect three different pieces of
331 evidence confirming our hypothesis on the mechanisms involved in scene segmentation.

332 First, by using RSA, we demonstrated that representational models built from fMRI
333 patterns show a significant correlation with isolated foreground in V2, V4 and LOC, while a
334 significant correlation with isolated background is achieved in V1 and V2 only.

335 Second, our analyses specifically found that foreground enhancement is present in all
336 the selected visual ROIs, and that this effect is driven neither by the foreground contrast, nor
337 by its size or location in the visual field. Thus, indirect evidence of figure-ground modulation
338 of natural images could be retrieved in the activity of multiple areas of the visual processing
339 stream (Roelfsema, 2006; Roelfsema and de Lange, 2016). This is consistent with a recent
340 study, which reported that border-ownership of natural images cannot be solved by single
341 cells, but requires a population of cells in monkey V2 and V3 (Hesse and Tsao, 2016).

342 Finally, a proof of segmentation can be represented by the significant suppression of
343 background-related information in V4 and LOC. On the contrary, earlier regions across the
344 visual stream - from V1 to V3 - have a uniform representation of the whole image, as evident
345 at first glance in the obtained correlation images (Figure 5). Overall these results further
346 support the idea that foreground enhancement and background suppression are distinct, but
347 associated, processes involved in scene segmentation of natural images.

348

349 **Foreground segmentation as a proxy for shape processing**

350 Of note, our proposed pre-filtering modeling approach produces a visual
351 representation (i.e., correlation image) of how information is selectively coded by a specific
352 population of interest (e.g., LOC). Further interpretations on the obtained visual
353 representation may result more empirical and, similarly to other computational neuroimaging
354 methods (e.g. Inverted Encoding Models: Liu et al., 2018), should be grounded on previous
355 neurophysiological knowledge. For instance, the correlation image of LOC could be
356 interpreted as resulting from two alternative mechanisms: LOC could preferentially process
357 the foreground as a whole, while suppressing the background, or it could act as a 'feature

358 detector', whose neurons are selectively tuned towards a single visual attribute (e.g., the
359 whiskers of a cat), without actively performing any suppression. Either way, what our method
360 clearly reveals is that LOC is selective for object texture and shape properties, and is
361 unaffected by background-related information. At the same time, previous knowledge
362 suggests that an active process, rather than a passive feature-matching mechanism,
363 determines the observed results (Roelfsema and De Lange, 2016).

364 Furthermore, the observed behavior of V4 and LOC is consistent with several
365 investigations on shape features selectivity in these regions, and in their homologues in
366 monkey (Carlson et al., 2011; Hung et al., 2012; Lescroart and Biederman, 2013; Vernon et al.,
367 2016). In fact, the extraction of shape properties requires segmentation (Lee et al., 1998), and
368 presumably occurs in brain regions where background is already suppressed. As mentioned
369 before, "correlation images" reconstructed from V4 and LOC are characterized by a strong
370 background suppression, while the foreground is preserved. This is consistent with a previous
371 neuropsychological observation: a bilateral lesion within area V4 led to longer response times
372 in identifying overlapping figures (Leek et al., 2012). Hence, this region resulted to be crucial
373 for accessing foreground-related computations, and presumably plays a role in matching the
374 segmented image with stored semantic content in figure recognition. In accordance with this,
375 a recent hypothesis suggests the role of V4 in high-level visual functions, such as features
376 integration or contour completion (Roe et al., 2012).

377 The preserved spatial resolution of foreground descriptive features (i.e., texture) in V4
378 and LOC – as shown in Figure 5 - represents an additional noteworthy aspect that arises from
379 our data. The progression from V1 towards higher-level regions of the cortical visual pathway
380 is associated with a relative increase in receptive fields size (Gattass et al., 1981; Gattass et al.,
381 1987; Gattass et al., 1988; Dumoulin and Wandell, 2008; Freeman and Simoncelli, 2011; Kay
382 et al., 2015). However, it should be kept in mind that regions such as V4 demonstrate a
383 complete representation of the contralateral visual hemifield, rather than selective responses

384 to stimuli located above or below the horizontal meridian (Wandell and Winawer, 2011). The
385 evidence that the foreground portion of “correlation images” maintains fine-grained details in
386 V4 and LOC seems to contrast a popular view according to which these regions are more
387 tuned to object shape (i.e., silhouettes), instead of being selective for the internal
388 configuration of images (e.g. Malach et al., 1995; Grill-Spector et al., 1998; Moore and Engel,
389 2001; Stanley and Rubin, 2003). However, it has been shown that foveal and peri-foveal
390 receptive fields of V4 do accommodate fine details of the visual field (Freeman and Simoncelli,
391 2011) and that the topographic representation of the central portion of this area is based on a
392 direct sampling of the primary visual cortex retinotopic map (Motter, 2009). Therefore, given
393 the “fovea-to-periphery” bias found in our stimuli and in natural images, it is reasonable that
394 an intact configuration of the foreground may be more tied to the activity of these brain
395 regions, and that a richer representation of the salient part may overcome simplistic models
396 of objects shape (e.g., silhouettes). Our results are also consistent with a recent study on
397 monkeys that demonstrates the role of V4 in texture perception (Okazawa et al., 2015).

398 Moreover, it is well known that selective attention represents one of the cognitive
399 mechanisms supporting figure segmentation (Qiu et al., 2007; Poort et al., 2012), as suggested,
400 for instance, by bistable perception phenomena (Sterzer et al., 2009), or by various
401 neuropsychological tests (e.g., De Renzi et al., 1969; Bisiach et al., 1976). In the present
402 experiment, participants were asked to simply gaze a central fixation point without
403 performing any overt or covert tasks related to the presented image. Nonetheless, we found
404 evidence of a clear background suppression and foreground enhancement, suggesting that
405 scene segmentation is mediated by an automatic process that may be driven either by bottom-
406 up (e.g., low-level properties of the foreground configuration), or top-down (e.g., semantic
407 knowledge) attentional mechanisms. Neurophysiological studies suggest that segmentation is
408 more likely a bottom-up process, as border-ownership assignment occurs as early as 70 ms
409 (Williford and von der Heydt, 2016), followed by later region-filling mechanisms (i.e.,

410 enhancement and suppression) (Self et al., 2013). A limit of our study is that we cannot
411 provide any further information related to these mechanisms and their temporal dynamics,
412 given the limited temporal resolution of fMRI and the passive stimulation task. However, a
413 recent study (Neri, 2017) investigated behavioral and electrophysiological responses to BSD
414 images - intact or manipulated in several different ways, including spatial frequencies filtering
415 and warping - in subjects who were asked to reconstruct a corrupted image region. Results
416 showed that reconstruction of patches elicits enhanced responses when masking targeted the
417 behaviorally segmented contours, rather than the contrast energy of the images. Moreover,
418 this effect occurs earlier than 100ms and is not altered by semantic processing or spatial
419 attention.

420

421 **Facing the challenge of explicit modeling in visual neuroscience**

422 One of the major goals of visual neuroscience is to predict brain responses in ecological
423 conditions (Felsen and Dan, 2005). In this sense, the standard approach in investigating visual
424 processing implies testing the correlation of brain responses from a wide range of natural
425 stimuli with features extracted by different alternative computational models. This approach
426 facilitates the comparison between performances of competing models and could ultimately
427 lead to the definition of a fully computable model of brain activity. However, the development
428 of explicit computational models for many visual phenomena in ecological conditions is
429 difficult. Indeed, many current theories, especially those concerning mid-level processing,
430 have been hardly tested with natural images, as testified by the extensive use of artificial
431 stimuli (e.g. Carandini et al., 2005; Wu et al., 2006). As a matter of fact, it is often impossible
432 both to extract and to control for relevant features in natural images, and thus, there is no way
433 to compute a predicted response from complex stimuli.

434 Moreover, even if computer vision is a major source of computational models and
435 feature extractors, often its objectives hardly overlap with those of visual neuroscience.

436 Computer scientists are mainly interested in solving single, distinct tasks (e.g., segmentation,
437 recognition, etc.), while, from the neuroscientific side, the visual system is considered as a
438 general-purpose system that could retune itself to accomplish different goals (Medathati et al.,
439 2016). Consequently, while computer science typically employs solutions that rely only
440 seldom on previous neuroscientific knowledge, and its goal is to maximize task accuracy (e.g.,
441 with deep learning), visual neuroscience somehow lacks of solid computational models and
442 formal explanations, ending up with several arbitrary assumptions in modeling, especially for
443 mid-level vision processing, such as scene segmentation or shape features extraction (for a
444 definition see: Kubilius et al., 2014).

445 In light of all this, we believe that the manipulation of a wide set of natural images, and
446 the computation of a fixed model based on low-level features, can offer a simple and
447 biologically plausible tool to investigate brain activity related to higher-order computations,
448 and that representational models offer an easily accountable link between brain activity
449 ~~patterns~~ and continuous stimuli descriptions (Nili et al., 2014). In fact, the results of this
450 exploratory approach can be depicted and are as intuitive as descriptions obtained through
451 formal modeling (Figure 5), highlighting interpretable differences rather than data
452 predictions.

453 Moreover, our study indicates that the sensitivity of representational models built on
454 fMRI patterns can represent an adequate tool to investigate complex phenomena through the
455 richness of natural stimuli. Representational models fit this purpose: even if are summary
456 statistics obtained from the dissimilarities between actual brain activity patterns, they are
457 independent from *a priori* assumptions on anatomical relationships between brain regions, or
458 on correspondences between voxels and units of computational models, as in the case of
459 voxelwise encoding or decoding (Kriegeskorte and Kievit, 2013).

460

461 **References**

- 462
- 463 Alexe B, Deselaers T, Ferrari V (2010) ClassCut for Unsupervised Class Segmentation. Lect Notes
464 Comput Sc 6315:380-393.
- 465 Arbelaez P, Maire M, Fowlkes C, Malik J (2011) Contour detection and hierarchical image
466 segmentation. IEEE Trans Pattern Anal Mach Intell 33:898-916.
- 467 Biederman I (1987) Recognition-by-Components - a Theory of Human Image Understanding.
468 Psychological Review 94:115-147.
- 469 Bisiach E, Capitani E, Nichelli P, Spinnler H (1976) Recognition of overlapping patterns and focal
470 hemisphere damage. Neuropsychologia 14:375-379.
- 471 Bosch A, Zisserman A, Munoz X (2007) Representing shape with a spatial pyramid kernel. In, pp
472 401-408: ACM.
- 473 Carandini M, Demb JB, Mante V, Tolhurst DJ, Dan Y, Olshausen BA, Gallant JL, Rust NC (2005) Do
474 we know what the early visual system does? J Neurosci 25:10577-10597.
- 475 Carlson ET, Rasquinha RJ, Zhang K, Connor CE (2011) A sparse object coding scheme in area V4.
476 Curr Biol 21:288-293.
- 477 David SV, Vinje WE, Gallant JL (2004) Natural stimulus statistics alter the receptive field structure
478 of v1 neurons. J Neurosci 24:6991-7006.
- 479 De Renzi E, Scotti G, Spinnler H (1969) Perceptual and associative disorders of visual recognition.
480 Relationship to the side of the cerebral lesion. Neurology 19:634-642.
- 481 Dumoulin SO, Wandell BA (2008) Population receptive field estimates in human visual cortex.
482 Neuroimage 39:647-660.
- 483 Efron B, Tibshirani R (1993) An introduction to the bootstrap. New York: Chapman & Hall.
- 484 Felsen G, Dan Y (2005) A natural approach to studying vision. Nat Neurosci 8:1643-1646.

- 485 Fowlkes CC, Martin DR, Malik J (2007) Local figure-ground cues are valid for natural images. *J Vis*
486 7:2.
- 487 Freeman J, Simoncelli EP (2011) Metamers of the ventral stream. *Nat Neurosci* 14:1195-1201.
- 488 Gattass R, Gross CG, Sandell JH (1981) Visual topography of V2 in the macaque. *J Comp Neurol*
489 201:519-539.
- 490 Gattass R, Sousa AP, Rosa MG (1987) Visual topography of V1 in the Cebus monkey. *J Comp Neurol*
491 259:529-548.
- 492 Gattass R, Sousa AP, Gross CG (1988) Visuotopic organization and extent of V3 and V4 of the
493 macaque. *J Neurosci* 8:1831-1845.
- 494 Grill-Spector K, Kushnir T, Edelman S, Itzhak Y, Malach R (1998) Cue-invariant activation in object-
495 related areas of the human occipital lobe. *Neuron* 21:191-202.
- 496 Handjaras G, Leo A, Cecchetti L, Papale P, Lenci A, Marotta G, Pietrini P, Ricciardi E (2017)
497 Modality-independent encoding of individual concepts in the left parietal cortex.
498 *Neuropsychologia* 105:39-49.
- 499 He K, Gkioxari G, Dollár P, Girshick R (2017) Mask r-cnn. arXiv preprint arXiv:170306870.
- 500 Hesse JK, Tsao DY (2016) Consistency of Border-Ownership Cells across Artificial Stimuli, Natural
501 Stimuli, and Stimuli with Ambiguous Contours. *J Neurosci* 36:11338-11349.
- 502 Hung CC, Carlson ET, Connor CE (2012) Medial axis shape coding in macaque inferotemporal
503 cortex. *Neuron* 74:1099-1113.
- 504 Huth AG, Nishimoto S, Vu AT, Gallant JL (2012) A continuous semantic space describes the
505 representation of thousands of object and action categories across the human brain.
506 *Neuron* 76:1210-1224.
- 507 Kastner S, De Weerd P, Ungerleider LG (2000) Texture segregation in the human visual cortex: A
508 functional MRI study. *J Neurophysiol* 83:2453-2457.

- 509 Kay KN, Naselaris T, Gallant JL (2011) fMRI of human visual areas in response to natural images.
510 CRCNS org.
- 511 Kay KN, Weiner KS, Grill-Spector K (2015) Attention reduces spatial uncertainty in human ventral
512 temporal cortex. *Curr Biol* 25:595-600.
- 513 Kay KN, Naselaris T, Prenger RJ, Gallant JL (2008) Identifying natural images from human brain
514 activity. *Nature* 452:352-355.
- 515 Khaligh-Razavi S-M (2014) What you need to know about the state-of-the-art computational
516 models of object-vision: A tour through the models. arXiv preprint arXiv:14072776.
- 517 Khaligh-Razavi SM, Kriegeskorte N (2014) Deep supervised, but not unsupervised, models may
518 explain IT cortical representation. *PLoS computational biology* 10:e1003915.
- 519 Kok P, de Lange FP (2014) Shape perception simultaneously up- and downregulates neural activity
520 in the primary visual cortex. *Curr Biol* 24:1531-1535.
- 521 Kriegeskorte N, Kievit RA (2013) Representational geometry: integrating cognition, computation,
522 and the brain. *Trends Cogn Sci* 17:401-412.
- 523 Kriegeskorte N, Mur M, Ruff DA, Kiani R, Bodurka J, Esteky H, Tanaka K, Bandettini PA (2008)
524 Matching categorical object representations in inferior temporal cortex of man and
525 monkey. *Neuron* 60:1126-1141.
- 526 Krizhevsky A, Sutskever I, Hinton GE (2012) Imagenet classification with deep convolutional neural
527 networks. In, pp 1097-1105.
- 528 Kubilius J, Wagemans J, Op de Beeck HP (2014) A conceptual framework of computations in mid-
529 level vision. *Front Comput Neurosci* 8:158.
- 530 Kubilius J, Bracci S, Op de Beeck HP (2016) Deep Neural Networks as a Computational Model for
531 Human Shape Sensitivity. *PLOS Comput Biol* 12:e1004896.
- 532 Lamme VA (1995) The neurophysiology of figure-ground segregation in primary visual cortex. *J*
533 *Neurosci* 15:1605-1615.

- 534 Lamme VA, Rodriguez-Rodriguez V, Spekreijse H (1999) Separate processing dynamics for texture
535 elements, boundaries and surfaces in primary visual cortex of the macaque monkey. *Cereb*
536 *Cortex* 9:406-413.
- 537 Lazebnik S, Schmid C, Ponce J (2006) Beyond bags of features: Spatial pyramid matching for
538 recognizing natural scene categories. In, pp 2169-2178: IEEE.
- 539 Lee TS, Mumford D, Romero R, Lamme VA (1998) The role of the primary visual cortex in higher
540 level vision. *Vision Res* 38:2429-2454.
- 541 Leek EC, d'Avossa G, Tainturier MJ, Roberts DJ, Yuen SL, Hu M, Rafal R (2012) Impaired integration
542 of object knowledge and visual input in a case of ventral simultanagnosia with bilateral
543 damage to area V4. *Cogn Neuropsychol* 29:569-583.
- 544 Lescroart M, Agrawal P, Gallant J (2016) Both convolutional neural networks and voxel-wise
545 encoding models of brain activity derived from ConvNets represent boundary-and surface-
546 related features. *J Vis* 16:756-756.
- 547 Lescroart MD, Biederman I (2013) Cortical representation of medial axis structure. *Cereb Cortex*
548 23:629-637.
- 549 Liu T, Cable D, Gardner JL (2018) Inverted Encoding Models of Human Population Response
550 Conflate Noise and Neural Tuning Width. *J Neurosci* 38:398-408.
- 551 Malach R, Reppas JB, Benson RR, Kwong KK, Jiang H, Kennedy WA, Ledden PJ, Brady TJ, Rosen BR,
552 Tootell RB (1995) Object-related activity revealed by functional magnetic resonance
553 imaging in human occipital cortex. *Proc Natl Acad Sci U S A* 92:8135-8139.
- 554 Marr D (1982) *Vision : a computational investigation into the human representation and*
555 *processing of visual information*. San Francisco: W.H. Freeman.
- 556 Medathati NVK, Neumann H, Masson GS, Kornprobst P (2016) Bio-inspired computer vision:
557 Towards a synergistic approach of artificial and biological vision. *Computer Vision and*
558 *Image Understanding* 150:1-30.

- 559 Miyawaki Y, Uchida H, Yamashita O, Sato M-a, Morito Y, Tanabe HC, Sadato N, Kamitani Y (2008)
560 Visual image reconstruction from human brain activity using a combination of multiscale
561 local image decoders. *Neuron* 60:915-929.
- 562 Moore C, Engel SA (2001) Neural response to perception of volume in the lateral occipital complex.
563 *Neuron* 29:277-286.
- 564 Motter BC (2009) Central V4 receptive fields are scaled by the V1 cortical magnification and
565 correspond to a constant-sized sampling of the V1 surface. *J Neurosci* 29:5749-5757.
- 566 Naselaris T, Kay KN, Nishimoto S, Gallant JL (2011) Encoding and decoding in fMRI. *Neuroimage*
567 56:400-410.
- 568 Neri P (2017) Object segmentation controls image reconstruction from natural scenes. *PLoS Biol*
569 15:e1002611.
- 570 Nili H, Wingfield C, Walther A, Su L, Marslen-Wilson W, Kriegeskorte N (2014) A toolbox for
571 representational similarity analysis. *PLoS Comput Biol* 10:e1003553.
- 572 Nishimoto S, Vu AT, Naselaris T, Benjamini Y, Yu B, Gallant JL (2011) Reconstructing visual
573 experiences from brain activity evoked by natural movies. *Current Biology* 21:1641-1646.
- 574 Ojala T, Pietikäinen M, Mäenpää T (2001) A generalized local binary pattern operator for
575 multiresolution gray scale and rotation invariant texture classification. In, pp 399-408:
576 Springer.
- 577 Okazawa G, Tajima S, Komatsu H (2015) Image statistics underlying natural texture selectivity of
578 neurons in macaque V4. *Proc Natl Acad Sci U S A* 112:E351-360.
- 579 Oliva A, Torralba A (2001) Modeling the shape of the scene: A holistic representation of the spatial
580 envelope. *International journal of computer vision* 42:145-175.
- 581 Poort J, Self MW, van Vugt B, Malkki H, Roelfsema PR (2016) Texture Segregation Causes Early
582 Figure Enhancement and Later Ground Suppression in Areas V1 and V4 of Visual Cortex.
583 *Cereb Cortex* 26:3964-3976.

- 584 Poort J, Raudies F, Wannig A, Lamme VA, Neumann H, Roelfsema PR (2012) The role of attention
585 in figure-ground segregation in areas V1 and V4 of the visual cortex. *Neuron* 75:143-156.
- 586 Qiu FT, Sugihara T, von der Heydt R (2007) Figure-ground mechanisms provide structure for
587 selective attention. *Nat Neurosci* 10:1492-1499.
- 588 Roe AW, Chelazzi L, Connor CE, Conway BR, Fujita I, Gallant JL, Lu H, Vanduffel W (2012) Toward a
589 unified theory of visual area V4. *Neuron* 74:12-29.
- 590 Roelfsema PR (2006) Cortical algorithms for perceptual grouping. *Annu Rev Neurosci* 29:203-227.
- 591 Roelfsema PR, de Lange FP (2016) Early Visual Cortex as a Multiscale Cognitive Blackboard. *Annu*
592 *Rev Vis Sci* 2:131-151.
- 593 Scholte HS, Jolij J, Fahrenfort JJ, Lamme VA (2008) Feedforward and recurrent processing in scene
594 segmentation: electroencephalography and functional magnetic resonance imaging. *J Cogn*
595 *Neurosci* 20:2097-2109.
- 596 Schreiber K, Krekelberg B (2013) The statistical analysis of multi-voxel patterns in functional
597 imaging. *PLoS ONE* 8:e69328.
- 598 Self MW, van Kerkoerle T, Super H, Roelfsema PR (2013) Distinct roles of the cortical layers of area
599 V1 in figure-ground segregation. *Curr Biol* 23:2121-2129.
- 600 Stanley DA, Rubin N (2003) fMRI Activation in Response to Illusory Contours and Salient Regions in
601 the Human Lateral Occipital Complex. *Neuron* 37:323-331.
- 602 Stanley GB, Li FF, Dan Y (1999) Reconstruction of natural scenes from ensemble responses in the
603 lateral geniculate nucleus. *J Neurosci* 19:8036-8042.
- 604 Sterzer P, Kleinschmidt A, Rees G (2009) The neural bases of multistable perception. *Trends Cogn*
605 *Sci* 13:310-318.
- 606 Thirion B, Duchesnay E, Hubbard E, Dubois J, Poline JB, Lebihan D, Dehaene S (2006) Inverse
607 retinotopy: inferring the visual content of images from brain activation patterns.
608 *Neuroimage* 33:1104-1116.

- 609 Vernon RJ, Gouws AD, Lawrence SJ, Wade AR, Morland AB (2016) Multivariate Patterns in the
610 Human Object-Processing Pathway Reveal a Shift from Retinotopic to Shape Curvature
611 Representations in Lateral Occipital Areas, LO-1 and LO-2. *J Neurosci* 36:5763-5774.
- 612 Wandell BA, Winawer J (2011) Imaging retinotopic maps in the human brain. *Vision Res* 51:718-
613 737.
- 614 Williford JR, von der Heydt R (2016) Figure-Ground Organization in Visual Cortex for Natural
615 Scenes. *eNeuro* 3.
- 616 Wu MC, David SV, Gallant JL (2006) Complete functional characterization of sensory neurons by
617 system identification. *Annu Rev Neurosci* 29:477-505.
- 618

619 **Legends**

620

621 **Figure 1. Comparing the Standard Modeling Approach and the Pre-Filtering Modeling Approach.**

622 A) In the standard modeling pipeline, different models are compared. After extracting
623 features from the stimuli, competing feature vectors can be used in order to predict brain
624 activity in an encoding procedure, whereas their dissimilarities can be used in a
625 representational similarity analysis. Finally, the model that better predicts brain responses is
626 discussed. B) In our pre-filtering modeling approach, different filtered versions of the original
627 stimuli are compared. Various biologically plausible filtering procedures are applied to the
628 stimuli prior to compute a unique feature space according to a given fixed and easily
629 interpretable model. In our approach a single model is employed and the step showing the
630 highest correlation with brain activity (or representational geometry) of each filtering
631 procedure is used to build a *post-hoc* “correlation image”. While the standard modeling
632 approach is theoretically more advantageous, as its output is a fully computable model of
633 brain activity, it can not be applied when reliable explicit models of perceptual processes do
634 not exist yet, as in the case of scene segmentation. Alternative attempts to reconstruct visual
635 stimuli from brain activity have been previously reported using multivariate techniques (e.g.
636 Stanley et al., 1999; Thirion et al., 2006; Miyawaki et al., 2008; Nishimoto et al., 2011).

637

638 **Figure 2. Analytical Pipeline.** A) Foreground enhancement test: the set of segmented stimuli is
639 tested against a null distribution of 1,000 permutations. Each permutation is built by
640 randomly shuffling the 334 behavioral foreground masks, and matching the root mean square
641 (RMS) contrast of the behaviorally segmented counterpart. This analysis controls for size,
642 location and contrast of the foreground when testing whether behavioral segmentations
643 explain each ROI representational dissimilarity matrix (RDM) better than chance. B)
644 Background suppression test: the correlation between brain RDMs and each step of the

645 background filtering procedure is tested against the correlation determined by the intact
646 stimuli. While information is filtered out, correlation can increase or decrease, depending on
647 the sensitivity for background related information in each ROI. A progressive decay indicates
648 that a region actually processes the background, while a significant increase suggests that
649 background is suppressed C) Filtering steps for the contrast or spatial frequencies filtering. D)
650 In clockwise order: features for each model were extracted from the stimuli; the dissimilarity
651 ($1 - \text{Pearson's } r$) between each stimulus pair was computed and aggregated in four RDMs; the
652 obtained RDMs were normalized in a 0-1 range; finally, the four RDMs were linearly combined
653 in the fixed model, which was then correlated to the fMRI RDM obtained from each ROI.

654

655 **Figure 3. Comparison of intact and behaviorally segmented images.** The graphs show the
656 correlation between the intact (green) and segmented versions (blue: isolated foreground;
657 red: isolated background) of the images and brain RDMs ($n = 55611$). Dashed bars stand for
658 significant correlations as resulting from the permutation test ($p < 0.05$, Bonferroni
659 corrected; 1000 iterations). Asterisks indicate significant differences between correlation
660 values ($p < 0.05$, Bonferroni corrected). Error bars represent the standard error estimated
661 with bootstrapping. Dashed lines represent the SNR estimate for each ROI, while gray shaded
662 regions indicate its standard error.

663

664 **Figure 4. Background Suppression in the Human Visual System.** Correlation between brain
665 activity and contrast, low- and high-pass filtering applied to the background (blue) and, as a
666 control, to the foreground (red). Filled dots mark significant correlations ($p < 0.05$,
667 Bonferroni corrected) while colored shaded areas represent the standard error estimates.
668 Dashed lines represent the SNR estimate for each ROI, while gray shaded regions indicate its
669 standard error. Arrows stand for significant differences ($p < 0.05$, Bonferroni corrected)
670 between each filtering step and correlation values for the intact version (up: background

671 suppression; down: progressive decay). Results show that for early regions (V1-3)
 672 background-related information is relevant, since the correlation significantly decays due to
 673 filtering ($p < 0.05$, Bonferroni corrected); on the other hand, V4 and LOC show an opposite
 674 effect, suggesting that background is suppressed in those regions.

675

676 **Figure 5. Correlation images.** To visually represent these results, we combined the different
 677 filtering procedures (contrast, low- and high-pass filtering) of the step showing the highest
 678 correlation with the representational model from each ROI.

679

680 **Table 1. Comparison of intact and behaviorally segmented images.**

ROI	Intact		Foreground		Background	
	Spearman's ρ	p-value	Spearman's ρ	p-value	Spearman's ρ	p-value
V1	0.091±0.008	< 0.001*	0.03±0.008	0.006	0.035±0.008	< 0.001*
V2	0.084±0.005	< 0.001*	0.035±0.007	< 0.001*	0.039±0.004	< 0.001*
V3	0.044±0.007	< 0.001*	0.025±0.008	0.08	0.02±0.007	0.29
V3A	0.023±0.004	0.34	0.017±0.005	0.256	0.018±0.007	0.127
V3B	0.036±0.009	0.017	0.028±0.006	0.02	0.017±0.009	0.186
V4	0.038±0.015	0.027	0.043±0.006	< 0.001*	0.013±0.007	0.915
LOC	0.038±0.008	0.015	0.038±0.012	< 0.001*	0.015±0.009	0.543

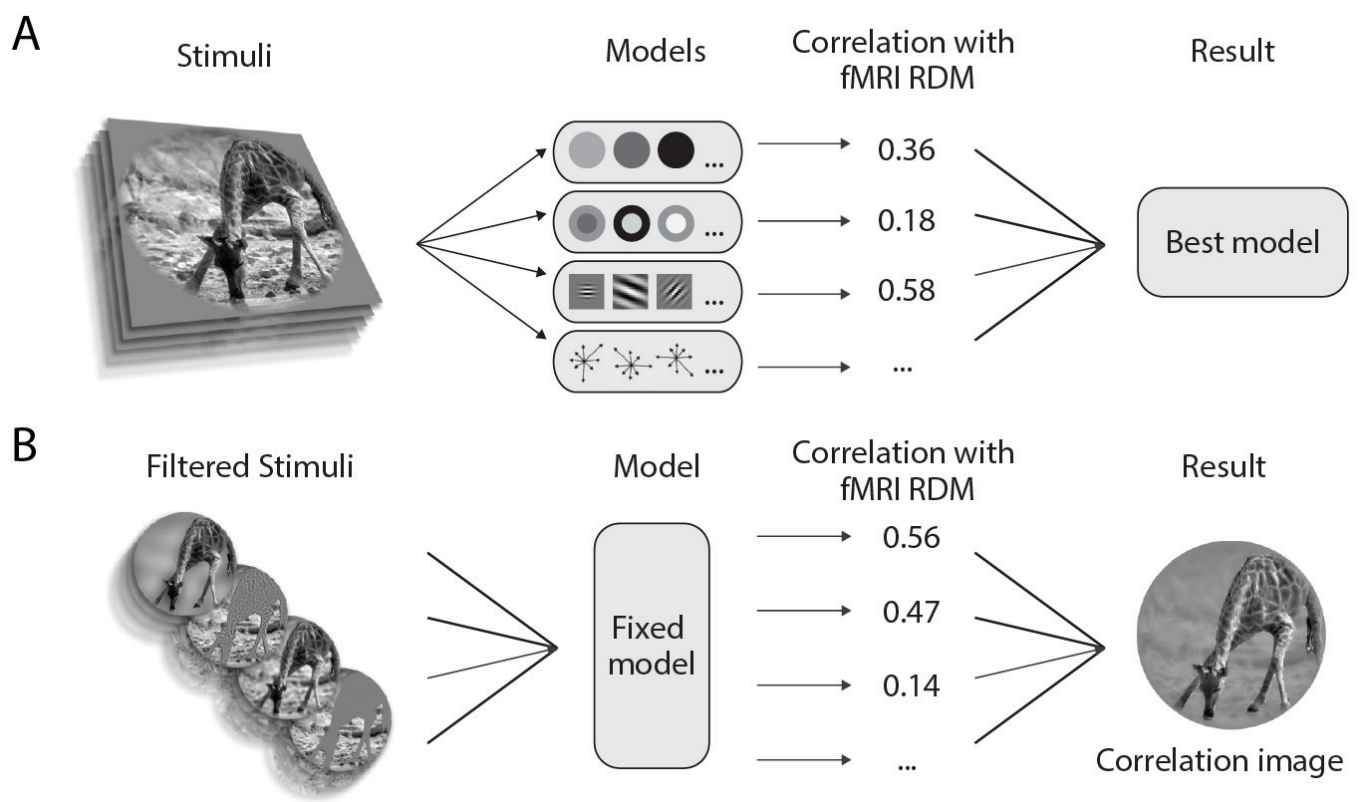
* = $p < 0.05$ Bonferroni corrected

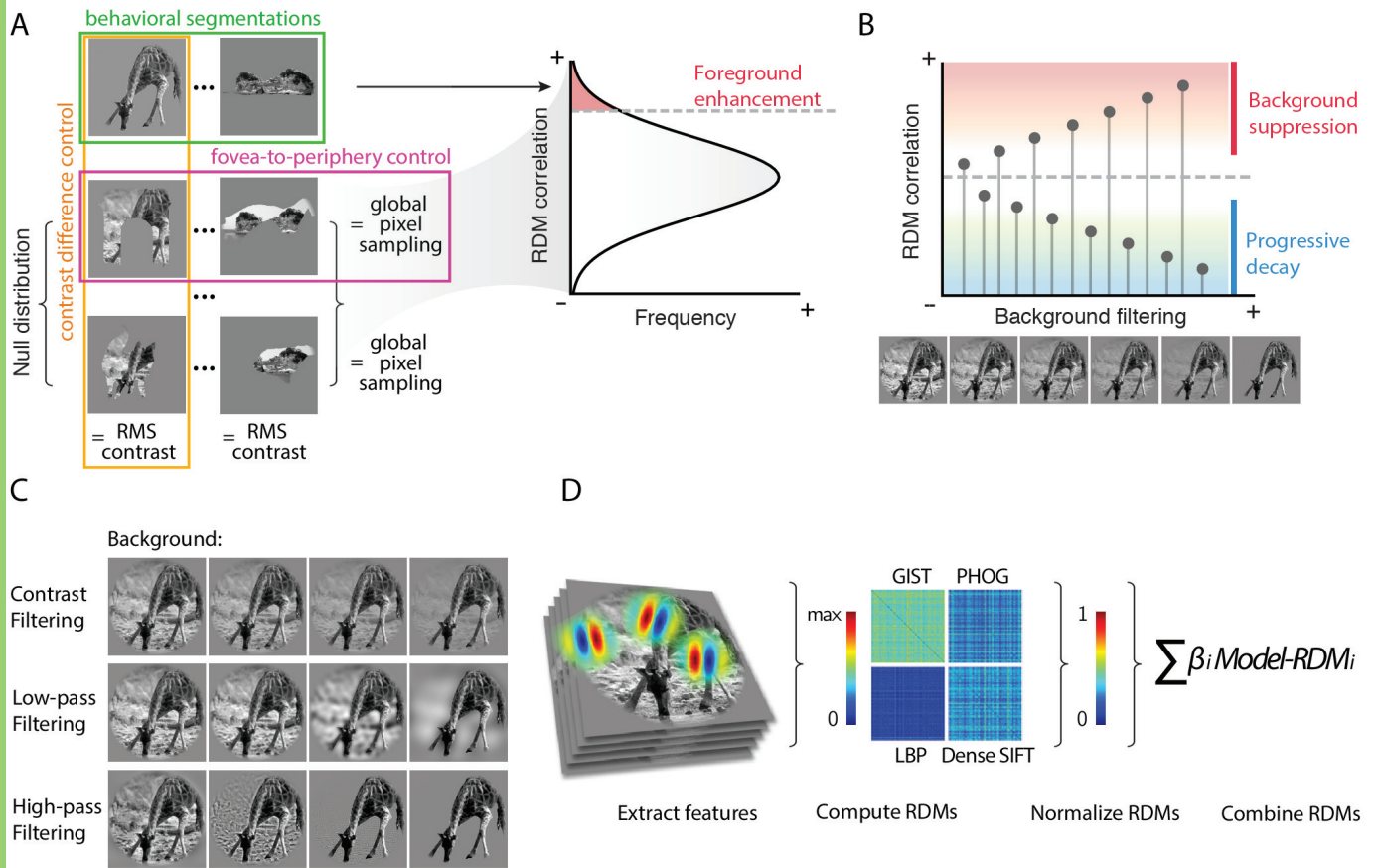
681

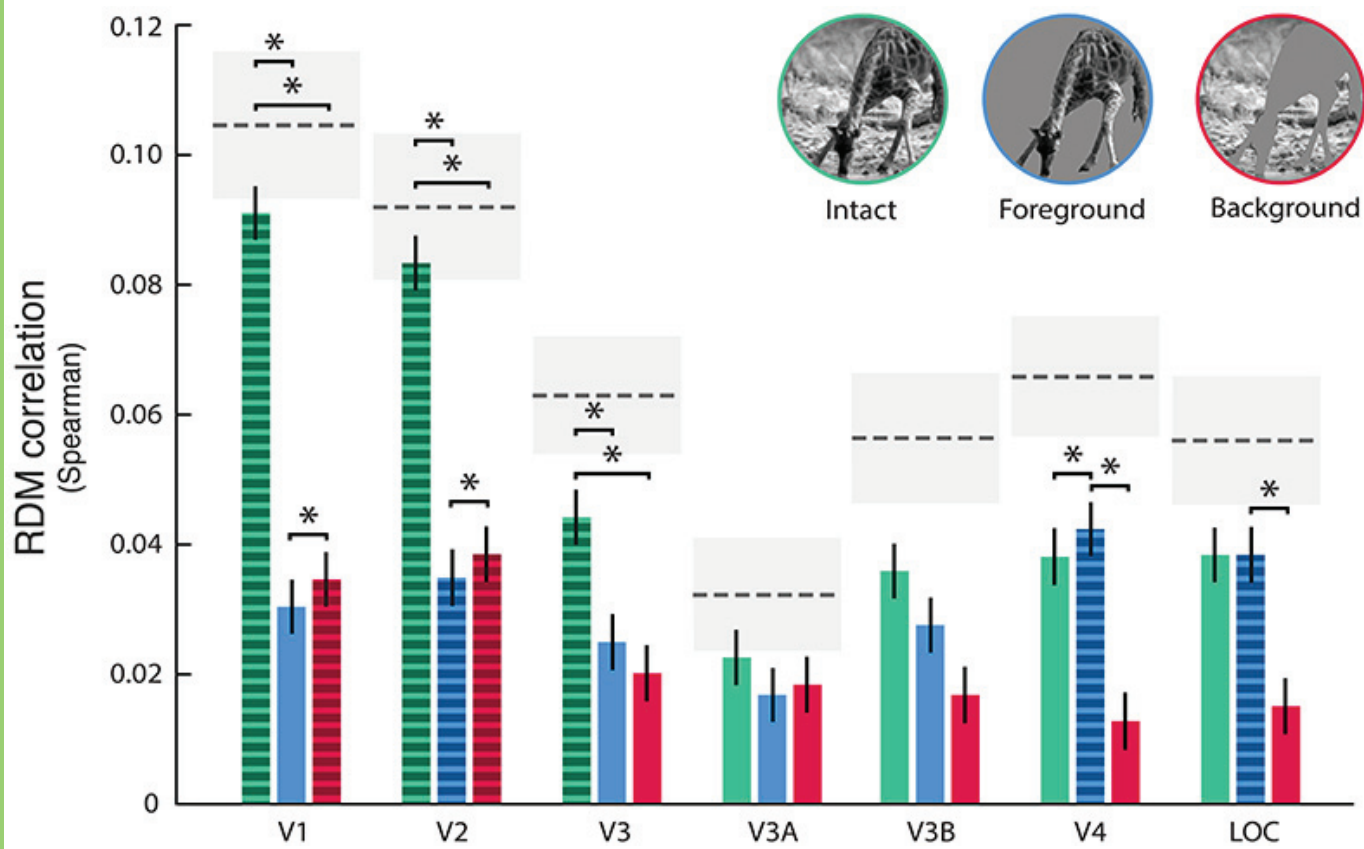
682 **Table 2. Statistical analysis**

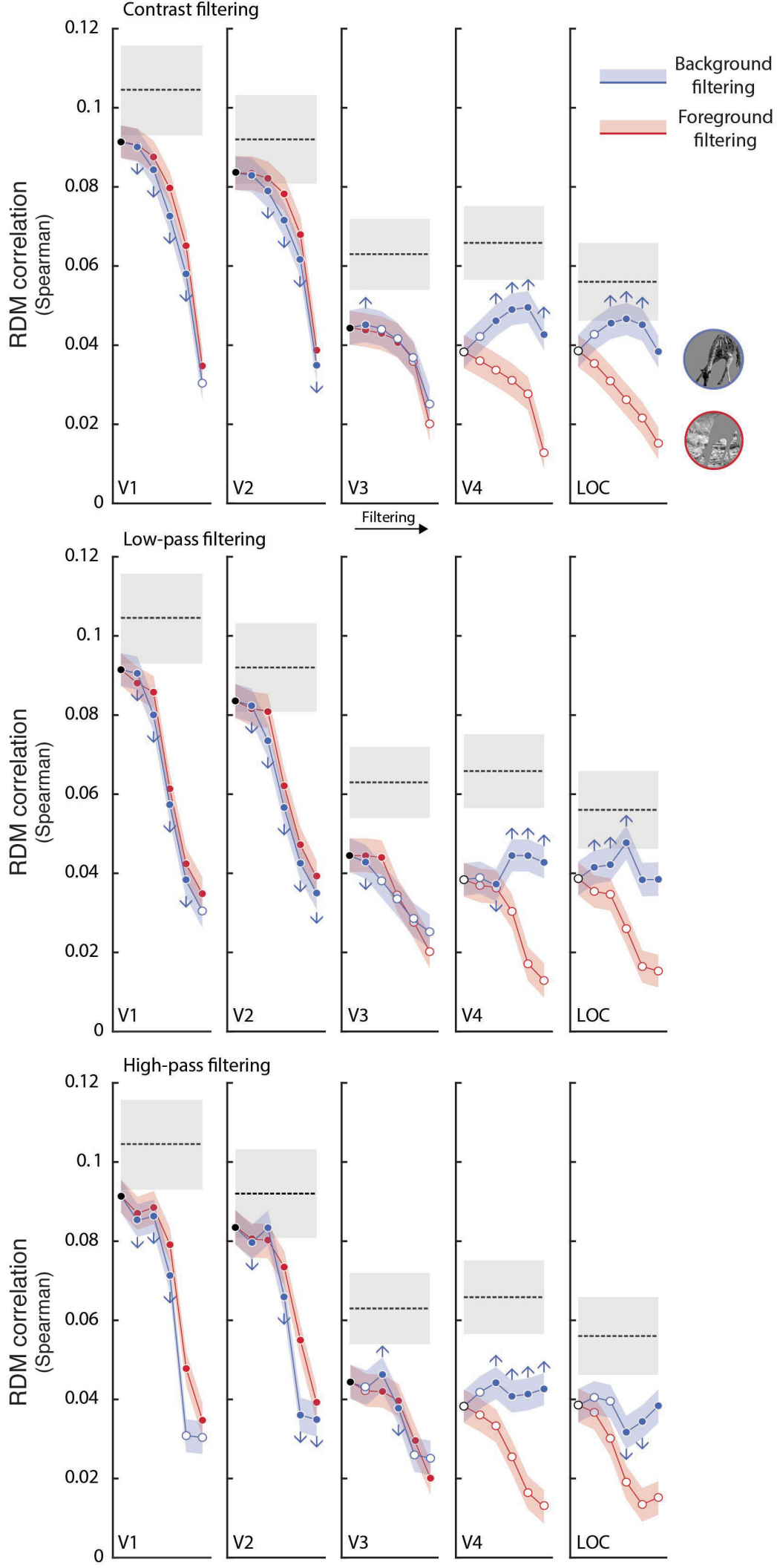
683

	Data structure	Type of test	Power
a	Single correlation values	Nonparametric permutation test	$p < 0.05$ Bonferroni corrected
b	Single correlation values	Nonparametric permutation test	$p < 0.05$
c	Single correlation values	Nonparametric permutation test	$p < 0.05$ Bonferroni corrected











V1



V2



V3



V4



LOC